AIP Advances

# Terahertz digital holography: Two- and four-step phase shifting technique in two plane image recording

Cite as: AIP Advances **11**, 105212 (2021); https://doi.org/10.1063/5.0062330
Submitted: 17 July 2021 . Accepted: 27 September 2021 . Published Online: 08 October 2021

Agnieszka Siemion, Linas Minkevičius, Domas Jokubauskis, et al.

# Terahertz digital holography: Two- and four-step phase shifting technique in two plane image recording

Cite as: AIP Advances 11, 105212 (2021); doi: 10.1063/5.0062330
Submitted: 17 July 2021 • Accepted: 27 September 2021 •
Published Online: 8 October 2021



Agnieszka Siemion,[1,a)] Linas Minkevičius,[2] Domas Jokubauskis,[2] Rusnė Ivaškevičiūtė-Povilauskienė,[2] and Gintaras Valušis[2]

## AFFILIATIONS

[1] Faculty of Physics, Warsaw University of Technology, 75 Koszykowa, Warsaw, Poland
[2] Department of Optoelectronics, Center for Physical Sciences and Technology, Saulėtekėo Ave. 3, LT-10257 Vilnius, Lithuania

[a)] **Author to whom correspondence should be addressed:** agnieszka.siemion@pw.edu.pl

## ABSTRACT

A two- and four-step phase shifting (PS) technique in terahertz (THz) digital holography is proposed. Relying on the Mach–Zehnder interferometer-based setup, it was demonstrated that the two-step and four-step PS in Fresnel holograms can assist in a five times greater background subtraction. It allows us to improve the quality of the obtained holographic images, in particular when objects introduce phase changes. It was shown that the recording of holograms of an object consisting of two separated planes can enable qualitative reconstruction of 3D images. Here, the planes were separated by 30 mm, thus defining the longitudinal (depth) resolution in this experiment. It is shown that the PS can serve in distinguishing transparent objects and, by a proper selection of phase variation within the 0–2$\pi$ range, enable us to increase the quality of the reconstructed hologram. Finally, the advantages of the suggested holographic technique are illustrated by comparing the results with the data of weak absorbing objects obtained via point-to-point, plane-to-plane (4$f$ setup), and dark-field THz imaging approaches. Experiments were performed at frequencies of 0.3 and 0.6 THz recording THz images using resonance antenna-coupled titanium microbolometers.



## I. INTRODUCTION

Terahertz (THz) holography is a rapidly developing investigation technique stimulated by a large variety of possible applications, in particular in discriminating weakly absorbing or transparent materials due to its high sensitivity to phase shifts. These features make digital holography very attractive for biological and medical investigations;[1,2] they open possibilities to increase image resolution,[3] either with additional autofocusing techniques[4] or performing the Fourier transform digitally,[5] or multiplexing facilities.[6]

Holographic images can be registered and reconstructed using a large variety of methods.[7] The so-called Fresnel hologram is a classical example of hologram, where the beam, diffracted by or at the sample, propagates to the hologram plane and interferes with the reference beam. The collimated beams—object $U_{object}$ and reference $U_{reference}$—impinging the hologram plane from the same side are mostly recorded at some angle.[7] Due to the fact that the intensity of the interference pattern is registered, the reconstruction results in the formation of four components in the Fourier domain: two phase-independent terms form a DC term (a zero frequency component) and two terms with the phase dependence form virtual and real images. In the case of digital holography, only the real image can be reconstructed and observed. Therefore, three other components form the unwanted noise in the image reconstruction, reducing its quality. There are different methods to alleviate this situation. One way is to exploit the filtration in the Fourier spectrum:[7] if the angle is wide enough, the reconstruction in a large enough calculation matrix will separate the components. However, such a method requires more numerical capacity, and due to the filtration, only part of the recorded information is used.

An alternative route to tackle the unwanted noise issue is to engage phase shifting (PS) methods.[8–10] The PS techniques are commonly used in digital holography to increase the quality of reconstructed images by reducing noise in the reconstructed intensity

distribution introduced by the beams that do not form the image. The technique utilizes multiple exposures and a special reconstruction algorithm to remove the spurious components from the image of the registered object.[11] In more details, mostly between two and five exposures are performed by recording consecutive holograms with the changed phase value of each reference beam. These particular phase shifts introduced in the reference beam in each exposure allow us to reconstruct the image via a particular algorithm.[12]

In this work, we demonstrate a novel PS approach in THz holography—two- and four-step PS technique—which enables a reconstruction of 3D objects via the introduction of different phase shifts in the reference beam. Here, we used two types of objects—first introducing amplitude and phase changes and second consisting of two separated planes in a space. Relying on the Mach–Zehnder interferometer-based setup and applying two-step and four-step phase shifts with the corresponding values equal to 0 and $\pi$ for the two-step method and 0, $\frac{\pi}{2}$, $\pi$, and $\frac{3\pi}{2}$ for the four-step method, it was demonstrated that the PS in Fresnel holograms can assist in a comprehensive unwanted background subtraction, thus improving the essential quality of obtained holographic images in two color—300 and 600 GHz—experiments. The experimental results have shown the average increase in contrast $(K)$ from 8.5 to 16.8 (Table I) and the decrease in the value of the background by a factor of 5 while reconstructing via a single hologram and the proposed two-step PS technique, respectively. In the case of four-step PS reconstruction, the contrast was not increased in relation to single hologram reconstruction and two-step PS; however, it should be noticed that all reconstructed parts of the image have a very similar contrast value. In other methods, they differ, while the object had uniform brightness.

The revealed improvement introduced by the usage of different phase-shifting techniques opens new possibilities to reconstruct the multi-plane images of recorded multi-plane weakly absorbing objects. It can be found well-suited for a large variety of applications, in particular in biology and biomedicine. Special attention should be given to the possibility to distinguish the phase levels of the investigated object that can be properly realized by the four-step PS method. The proposed in-line holographic systems with the phase-shifting technique allow us to increase the information capacity in the optical system. Moreover, we demonstrated the dual-wavelength recording of a two-plane object and its successful reconstruction in both planes.

## II. THEORETICAL FRAME FOR TWO- AND FOUR-STEP PS TECHNIQUES IN THz HOLOGRAPHY

Registering and reconstruction of digital holograms can be realized in many different ways[7] employing the features of optical setup geometry, properties of sources, or reconstruction techniques.

Interferometer principle-based setups are convenient for alignment and use; moreover, such a geometry allows us to reach a very small—close to 0°—angle between the interfering beams. However, in this case, the reconstructed components, corresponding to the DC term and real and virtual images, overlap,[13] which causes a reduction in the quality of the reconstructed image due to the increased background noise. This arises from the light field distribution in the real image plane coming from the virtual image and the DC term. Therefore, it is of a particular need to suppress this negative influence.

In what follows, we propose a step PS technique to resolve the issue of the noise subtraction and proper determination of phase distribution in the sample. More specifically, we introduce the two-step and four-step PS technique corresponding to the phase shifts in the reference beams equal to 0 and $\pi$ for the two-step technique and 0, $\frac{\pi}{2}$, $\pi$, and $\frac{3\pi}{2}$ for the four-step technique.

The intensity pattern recorded for a single hologram can be described as follows:

$$I_{hologram}(x,y) = |U_{object}(x,y) + U_{reference}(x,y)|^2, \tag{1}$$

where $U_{object}$ describes the light field distribution in the hologram plane $(x,y)$ coming from the object beam and $U_{reference}$ is the reference beam in the hologram plane (with or without a phase shift).

In the four-step case, four different holograms are recorded (each with different phase shifts introduced in the reference beam). The calculated complex transmittance reconstructing the light field distribution propagating back to the real image plane can be described using the following equation:

$$T_{hologram-PS4}(x,y) = \sum_{j=1}^{j=4} I_j(x,y) U_{reference\_j}(x,y), \tag{2}$$

where $I_j$ is the intensity of the hologram recorded for each exposure and $j$ is the consecutive number corresponding to different phase shifts introduced in each reference beam $U_{reference\_j}$ and is equal to 0, $\frac{\pi}{2}$, $\pi$, and $\frac{3\pi}{2}$ for $j = 1, 2, 3,$ and 4, respectively. The complex

**TABLE I.** Contrast values for simulation results and experimentally reconstructed image (calculated from the intensity distribution) for two areas of the "E" letter in one plane—with constant phase distribution (right letter) and various phase levels inside (left letter).

| Contrast | | Single hologram | PS2 | PS4 |
|---|---|---|---|---|
| Simulations (large aperture) (Fig. 2) | Right "E" | 8.85 | 25.00 | 14.85 |
| | Left "E" | 4.17 | 25.06 | 16.80 |
| Simulations (small aperture) (Fig. 3) | Right "E" | 3.60 | 1.07 | 5.55 |
| | Left "E" | 3.02 | 13.86 | 7.69 |
| Experiment (Fig. 7) | Right "E" | 8.54 | 16.76 | 6.03 |
| | Left "E" | 10.66 | 11.33 | 6.51 |

reference beam is a plane wave for each hologram having a different phase value. Thus, the term $U_{reference\_j}(x,y)$ can be simplified to $1, i, -1$, and $-i$ in the summation. Therefore, Eq. (2) can be rewritten as follows:

$$T_{hologram-PS4}(x,y) = I_1(x,y) - I_3(x,y) + i[I_2(x,y) - I_4(x,y)]. \quad (3)$$

We must recall that each $I_i(x,y)$ distribution consists of four components. Two of these components form a DC term that is not phase-sensitive, and the other two are real and virtual images. Furthermore, all these 4 exposures are multiplied by the value corresponding to the phase shift of the reference beam, and we obtain 16 components that can be simplified as follows:

$$T_{hologram-PS4}(x,y) = 4U_{object}(x,y), \quad (4)$$

which, after the back propagation (to the real image plane), will reconstruct only the light field distribution related to the real image.

In the case of the two-step technique, only two exposures are registered for the phase shift of the reference beam equal to 0 and $\pi$, and the resulting transmittance can be written as follows:

$$T_{hologram-PS2}(x,y) = I_1(x,y) - I_3(x,y). \quad (5)$$

In this case, there are eight different components, and after the multiplication with the corresponding phase shifts of the reference beams, we obtain

$$T_{hologram-PS2}(x,y) = 2U_{object}(x,y) + 2U^*_{object}(x,y), \quad (6)$$

where $^*$ is the complex coupling operation, and thus, $U^*_{object}$ describes the light field distribution forming the virtual image. As it is seen, the unwanted $U^*_{object}$ component is not removed in this technique. However, it should be mentioned that the transmittance $T_{hologram-PS2}(x,y)$ is propagated to the real image plane where the real image is sharp and well defined, while the light field distribution corresponding to the virtual image forms a divergent beam that only slightly affects the background. The background is lighter; however, it introduces noise. Nevertheless, in comparison with the noise introduced by the DC term component, the noise introduced by $U^*_{object}$ is hardly noticeable. It is worth noting that the two-step technique is two times faster due to the fact that it requires only two exposures instead of four used in a previous approach.

To illustrate the proposed approach, a special sample, consisting of two "E" letters of different types, was constructed. The sample design is shown and commented in Fig. 1. It should be noticed that the opening thickness in "E" letters is equal to 7 mm, which corresponds only to 7 wavelengths in the case of using the 300 GHz beam and 14 wavelengths for the 600 GHz beam.

The comparison between the different recording and reconstructing methods is illustrated in Fig. 2. One can note that in these simulations, the single "E" letter forming the object was 90 mm in height and 60 mm in width, i.e., two times larger than in the experiment (to additionally reduce possible large diffraction effects on the letters). It was assumed that two beams interfere in the hologram plane at an angle of 0°. The simulation parameters were as follows: the distance between the object and the hologram plane was equal to 85 mm, and the recording and reconstructing wavelength was chosen to be 0.5 mm (equivalent to the experimental frequency of

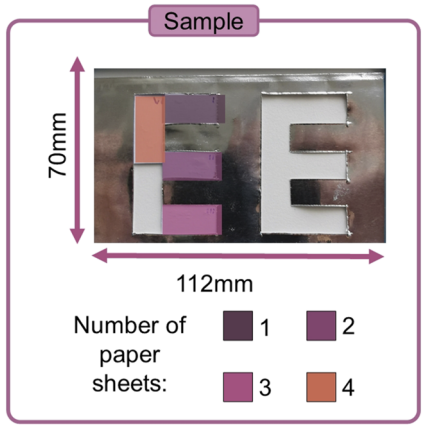


**FIG. 1.** Specially designed sample to illustrate the two- and four-step PS techniques in THz holography. The sample was fabricated from the aluminum foil of dimensions of 70 × 112 mm$^2$ with cut-out "EE" shape elements inside. The left "E" letter consisted of five areas dedicated to produce different phase shifts 0, $\frac{\pi}{4}$, $\frac{\pi}{2}$, $\frac{3\pi}{4}$, and $\pi$ for 600 GHz corresponding to 0, 1, 2, 3, and 4 paper sheets that are indicated by different colors. The right "E" letter was "empty" and served as a reference. This sample was illuminated with a quasi-plane wave and formed the object beam.

600 GHz). The calculation matrix was 2048 × 2048 pixels with the sampling equal to 0.3 mm that corresponded to a square area of 614.4 mm. Such a relatively large calculation matrix was chosen to diminish the edge effects and limited aperture influence.

As a reference, the intensity and phase distributions of the image reconstructed by the classic back propagation method (Angular Spectrum of Plane Waves—ASoPW) were calculated. The results are shown in Figs. 2(a) and 2(d). The light field corresponding to the

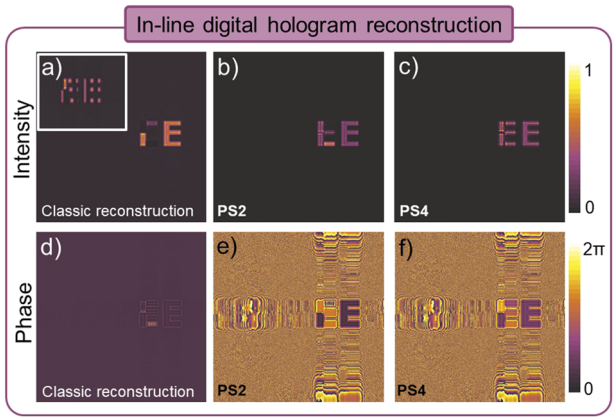


**FIG. 2.** Numerical simulations illustrating the differences between the reconstruction of the THz Fresnel hologram using different methods: (a) and (d) classic back propagation (using the angular spectrum of plane waves method), (b) and (e) two-step PS method, and (c) and (f) four-step PS method. (a)–(c) depict the intensity distributions, while (d)–(f) depict the corresponding phase distributions. The intensity pattern of the reconstructed image in the case of a small (1°) angle between the interfering beams is presented in the inset of (a) for illustration. Note the expressed characteristic sine-like interference pattern here.

DC term component is clearly visible, forming a uniform and noticeable background, which is not observed in other cases [see Figs. 2(b), 2(c), 2(e), and 2(f)]. As it is seen from the hologram reconstruction in Fig. 2(a), the reconstructed image is formed by two reconstructed beams corresponding to the object and reference. They propagate numerically along the same optical axis and overlap in the real image plane, making the reconstructed image not reliable. Inside the left "E" letter, bright and dark regions can be seen instead of uniform distribution as it was in the object. The intensity distribution is changed due to the different phase values of the object, and such an intensity distribution corresponds to the interference pattern. To illustrate this fact more thoroughly, an additional simulation was created with an angle of 1° between the beams, and in the inset of Fig. 2(a), the characteristic sine-like interference pattern is present.

In the THz range, many objects can be transparent and thus introduce a particular phase shift. Such features of the object result in the reconstructed interference pattern of two beams. It can also be clearly seen in the inset of Fig. 2(a) where an additional interference pattern appears even when an angle of 1° between the recorded beams is introduced. The numerical reconstruction does not take into account the presence of a beam splitter; thus, we observe such an effect. For visible light, most of the objects are diffusive, which means that their phase distribution is random. Therefore, the components (DC term and real and virtual images) would overlap, but there would be no interference fringes as it is visible in Fig. 2(a). As it was already mentioned, the two-step PS technique [Fig. 2(b)] removes only the influence of the DC term. As a result, an interference of real image reconstruction with the light field distribution formed as the divergent beam resulting from the virtual image creates an interference pattern in the left "E" letter. The background is significantly smaller than for classic reconstruction and is similar to that for the four-step PS technique [Fig. 2(c)].

One can note that the four-step PS technique ideally reconstructs the information about the intensity [Fig. 2(c)] and phase [Fig. 2(f)] of the object. Note the visible diffraction effects on the edges of the object. It must be underlined that in the case of phase retrieval methods, the four-step PS technique is preferable regardless of two times larger registering time. However, in the case of absorbing and not transparent objects, the two-step technique can give reasonable enough results, and it is two times faster. To remove the unwanted background, it is enough to apply the two-step PS algorithm; however, to reconstruct proper information about phase shifts introduced by the object, the four-step PS algorithm needs to be used. Thus, the two-step PS technique is beneficial in the case of absorbing objects, i.e., mainly intensity change related images, while the four-step technique is more preferable in the studies of low-absorbing or transparent objects relying on the phase changes.

After the illustration of the technique, a set of simulations was conducted corresponding to the real experimental conditions. The real object was smaller in comparison to that used in illustrating simulations given in Fig. 2—in the experiment, "E" letters were of 45 mm height and 30 mm width. The calculation matrix was 1024 × 1024 pixels (each having a size of 150 × 150 $\mu m^2$, resulting in the area of 153.6 mm-edge-size-square). Moreover, the left "E" letter was divided into five different areas to induce different phase shifts: 0, $\frac{\pi}{4}$, $\frac{\pi}{2}$, $\frac{3\pi}{4}$, and $\pi$ corresponding to 0, 1, 2, 3, and 4 paper sheets (for 600 GHz radiation). It was also assumed that two beams interfere in the hologram plane at an angle of 0° [for classic reconstruction

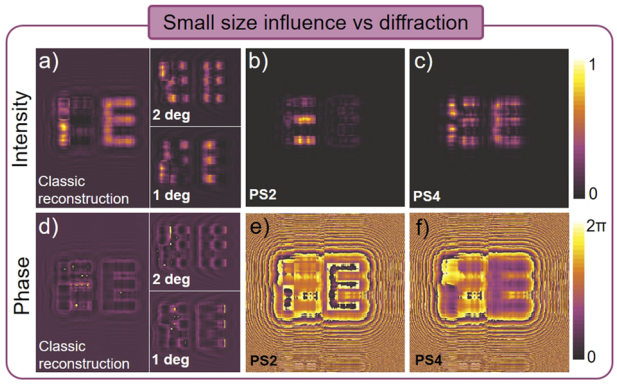


**FIG. 3.** Numerical simulations illustrating diffraction effects resulting from a small size of the object in comparison with the wavelength. Simulation parameters correspond to real experimental conditions. Reconstruction of the THz Fresnel hologram using different methods: (a) and (d) classic back propagation (using Angular Spectrum of Plane Waves—ASoPW), (b) and (e) two-step PS technique, and (c) and (f) four-step PS technique. (a)–(c) show the intensity distributions. (d)–(f) depict the corresponding phase distributions. The intensity and phase patterns of the reconstructed image in the case when small (1° and 2°) angles between the interfering beams are introduced are shown in the insets of (a) and (d). Note the pronounced characteristic interference pattern.

also at 1° and 2°, showing the influence of misalignment—insets of Figs. 3(a) and 3(d)]. The simulation parameters correspond to the values in the experiment. The distance between the object and the hologram plane was kept equal to 85 mm, and the recording and reconstructing wavelength was of 0.5 mm (600 GHz).

As it is seen from Fig. 3, a strong influence of diffraction effects is clearly noticeable.[14] The interference of two reconstructed beams in classic [Figs. 3(a) and 3(d)] and two-step PS [Figs. 3(b) and 3(e)] methods is evident. Moreover, misalignment-induced effects in the experimental setup are illustrated in the insets of Figs. 3(a) and 3(d). They manifest themselves as a characteristic stripe-like pattern resulting from the interference of two beams.

The resolved difference can be observed in the reconstructed phase distributions. The classic hologram approach does not give a proper mapping of the phase values introduced by the object. In the case of classic in-line digital holography, two beams—object and reference—are simultaneously reconstructed and overlap in the image plane, forming an interference pattern. Thus, the reconstructed light field distribution is not the exact amplitude and phase distribution introduced only by the object, which can be seen as dark areas in the reconstructed intensity distribution in the image of "EE" letters in Figs. 2(a), 2(b), 3(a), and 3(b). Hence, the best solution is to use the four-step PS technique illustrated in Figs. 2(c) and 2(f), which allows us to remove all unwanted reconstruction components, according to Eqs. (3) and (4). Using multiple exposures with different phase shifts of the reference beam allows us to reconstruct (from the numerically changed hologram) only the information about the object without additional components, forming noise. This approach allows us to properly reconstruct phase values introduced by the object. The two-step PS method [Figs. 2(b) and 2(e)] introduces the additional piston-like phase value resulting from the divergent field that shifts all phase values. Nevertheless, all differences introduced as the object phase shifts are distinguishable. The

intensity pattern suffers from the effect of interference of two reconstructed beams, forming the real and virtual images; however, the phase distribution is reconstructed properly.

The two-step and four-step PS techniques require an interferometric registering optical setup and give good quality reconstructed images. One can note that the two-step PS is faster, while the four-step provides better image quality, especially in the case of imaging phase objects. To quantitatively compare the obtained results, contrast values ($K$) defined as $K = \frac{I_{av}(s)-I_{av}(n)}{I_{av}(n)}$ were calculated. Here, $I_{av}(s)$ and $I_{av}(n)$ are the average intensity values corresponding to the signal area and the background noise area. The contrast values calculated from simulations and experimental results for object introducing phase changes characterized by variable intensity values are given in Table I and are strongly dependent on the phase level introduced by the object. It should be underlined that comparing parameters related to the intensity distribution (like contrast $K$) of the hologram of the phase object can be misleading while relating to the single areas. It is obvious that for two uniformly illuminated areas with introduced phase shifts of 0 and $\pi$, maximal and minimal intensity values, corresponding to positive and negative interferences, respectively, will be observed. The values of $K$ in the case of the experimental four-step PS technique are smaller than those for the two-step PS technique. Moreover, it should be underlined that the contrast of left and right "E" letters has the same values only for the four-step PS technique. Hence, only this technique (totally reducing all other hologram components) gives the assumed intensity distribution of the transparent object with introduced phase shifts. However, the phase values obtained only from the four-step PS technique correspond well to those introduced by the object; hence, this approach can successfully be used to map the phase objects properly. This illustrates also better fidelity of the intensity imaging in the case when the object introduces phase changes.

One of the essential points is the background subtraction by introducing PS techniques. The noise level was calculated as the average intensity value in the background area of reconstructed images. It is enough to use the two-step PS technique to reduce the noise level from 0.051 (calculated from single hologram reconstruction; Fig. 3) to 0.010 in simulations and from 0.034 to 0.017 in the experiment.

## III. EXPERIMENTAL SETUP

The experimental optical setup based on the Mach–Zehnder interferometer is presented in Fig. 4. It is based on Schottky diode-based frequency multiplier chains delivering the THz radiation of 0.3 and 0.6 THz frequencies.

The delivered coherent radiation is collimated by passing the converging lens (L1, with $f$ = 12 cm). Then, after the reflection by gold-coated mirror M1, the collimated THz beam is divided into two parts by beam splitter BS1 with a ratio of 1:1 and enters into the interferometric part. One part of the beam is reflected from mirror M2, and then, it is phase shifted by the introduced element PS and reaches beam splitter BS2 (thus forming the reference beam). The other part of the beam is reflected by mirror M3, passes through the object (sample), and reaches BS2 (forming the object beam). Then, both beams reunite, and from that time, they propagate along the same optical axis, reaching the detector. The intensity of the interference pattern is registered using a high performance antenna-coupled

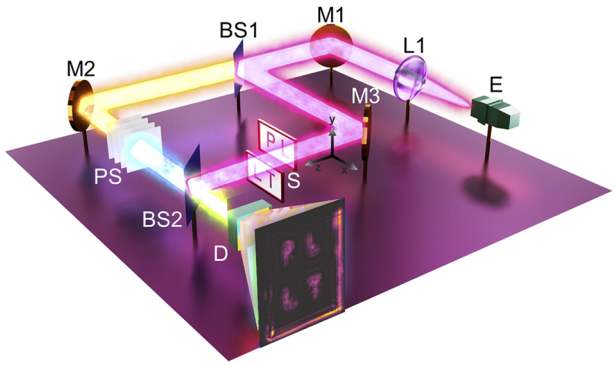


**FIG. 4.** Principal scheme of the optical setup used to record a THz digital hologram at 0.3 and 0.6 THz. Letter "E" denotes the electronic THz emitter; L1 is the high-density polyethylene (HDPE) lens with $f$ = 12 cm; M1, M2, and M3 are gold-coated flat mirrors with a diameter of 50 mm; BS1 and BS2 label high resistivity silicon beam splitters (525 $\mu$m thickness, with both sides polished); S (sample) is the object with "LT" and "PL" shape apertures in the aluminum sheet; PS is a phase shifter—different amounts of paper sheets introducing particular phase shifts in the reference beam; and D is a titanium-based microbolometric detector. The example of the image reconstructed from the registered hologram of "PL" and "LT" samples is shown behind the detector.

titanium microbolometer[15] working at room temperature. To alleviate the influence of the small-aperture-size optical elements, the detector was placed in the main optical axis, and the object was shifted by a computer controlled motorized *xyz* axis stage. Such a solution allowed us to record the interference pattern resulting from two overlapping beams in the middle of the optical setup where the diffraction effects are not critical. Moreover, in such a case, the phase value in the reference beam remains constant for the whole hologram and is free from diffraction effects.

## IV. TWO-PLANE-OBJECT RECONSTRUCTION FOR TWO DIFFERENT FREQUENCIES

There are several propagation techniques that can be employed in the reconstruction process of THz holograms. One can use the Fresnel diffraction method,[7,16] or if the recording is made in different conditions, the Fourier transform method can be suitable.[5,7]

We preferred, however, the ASoPW method as it contains no approximations and assures proper sampling conditions; moreover, it is relatively free of numerical errors.[17] This technique allows us to access and modify the hologram digitally in its complex distribution, and also, it enables us to introduce changes in its spatial frequency domain (Fourier spectrum). The angular spectrum method relies on the assumption that any light field distribution can be decomposed into individual plane waves traveling at different directions. These plane waves combine to create a complex light field distribution, such as a diffractive element, a hologram. After decomposition into individual plane waves, these plane waves can be digitally propagated at a distance $z$ to recover the complex light field at any other location in space.[7] The propagation of the plane wave is simple as it has uniform amplitude and phase value changing as the sine function together with the propagation distance.

In this section, a reconstruction of two 2D objects separated by some distance was conducted. The hologram of the object composed of two planes was recorded and formed a single hologram that was

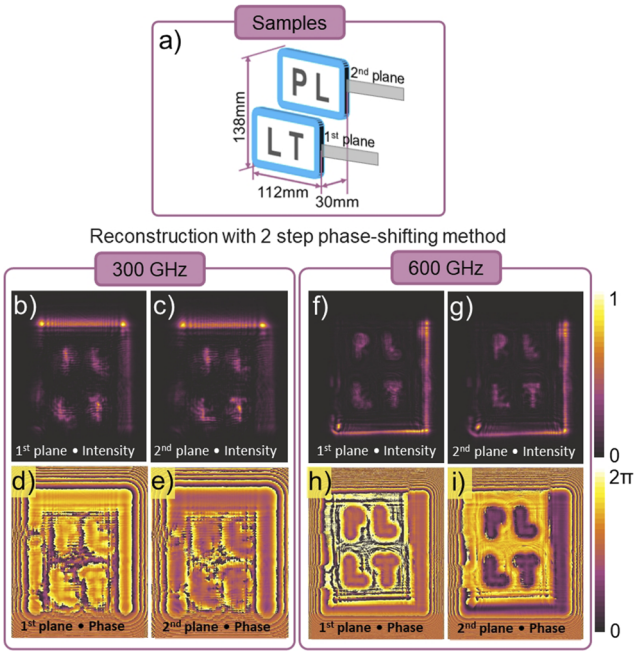


**FIG. 5.** Two 2D object reconstruction for two different frequencies using the PS technique and ASoPW propagation method. (a) Scheme of the object that consists of two 70 × 112 mm$^2$ aluminum foil sheets. The first sample has a cut-out "LT" shape element and was placed in the first plane (85 mm from the hologram plane), which is closer to BS2. The second sample has a cut-out "PL" shape element and was placed in the second plane (115 mm from the hologram plane). Samples are separated by a gap of 30 mm and are shifted vertically, so they do not overlap (such geometry results from the small size of the letters with respect to the used wavelength and the absence of the diffuser in the recording process). The intensity distributions of the reconstructed images in the first and second planes are shown in (b) and (c) for 300 GHz and (f) and (g) for 600 GHz. The corresponding phase distributions in the mentioned planes are shown in (d) and (e) for 300 GHz and (h) and (i) for 600 GHz.

reconstructed later. Figure 5 shows two-plane-object reconstruction for two different frequencies using the two-step PS technique and ASoPW propagation method.

Thus, two sets of transparent letters—"LT" and "PL"—were mounted at two different distances—85 and 115 mm—from the hologram plane. In the case of the two-step PS technique, two holograms were recorded for two different phase shifts of the reference beam, 0 and $\pi$, respectively. Moreover, such a set of holograms was recorded for the frequencies 300 and 600 GHz, which also enables heterodyne reconstruction.[18]

The better image resolution and reconstruction are obtained for higher frequency as expected. However, one needs to note that the width of the slits in "LT-PL" letters was equal to 5 mm (the height of the letter is equal to 30 mm), which corresponds to only five and ten wavelengths for each frequency, respectively. In 300 GHz reconstructed images, significant diffraction effects are visible. As one can see, numerical simulations that were conducted for the "EE" sample (presented in Fig. 3) should be free from any imperfections existing in real experimental conditions. The presented simulation data are characterized by a strong diffraction influence even though simulations are conducted at two times larger frequency.

The image was reconstructed at two distant planes using the phase-shifting technique (Fig. 5) and single hologram reconstruction given in Fig. 11 of the Appendix. The uniform phase distribution inside "LT-PL" letters is consistent with the theory and our predictions. In this experiment, no additional phase shifts were introduced inside the sample.

Single hologram reconstruction has almost no information about the phase, while in the PS technique, the contours of letters are visible and the inside of the letter has a uniform level of phase—the same in all letters but different in different image planes. Single hologram reconstruction can give similar intensity distribution as the phase-shifting technique, but in the case of the particular phase shift of the reference beam—here used for PS reconstruction—it can change the reconstructed image. As it can be seen in Fig. 11 (right), the letter area is darker than the background, which is caused by the $\pi$ shift in the reference beam. Such reconstruction is characterized by the negative values of contrast related to the contrast inversion. Thus, such reconstruction is not proper. In the case of using PS techniques, the intensity image is clear and has better contrast than the image reconstructed from the single hologram (in the case of normal and inverted images). The contrast values calculated for each letter area in two image planes are given in Table II. These values correspond to experimental data, and it can be seen that single hologram reconstruction is characterized by the decreased contrast value by ~90% in comparison to the PS technique for the first plane and 70% for the second plane at 300 GHz.

**TABLE II.** Contrast values for reconstructed images (calculated from the intensity distributions) for two planes (with "PL" and "LT" letters distant 30 mm from each other) and two frequencies—300 and 600 GHz. The minus sign corresponds to the inverted contrast—it means that the background is brighter than the letter area—see Fig. 11.

| | | 300 GHz | | | 600 GHz |
|---|---|---|---|---|---|
| | | One hologram | | | |
| Contrast | | No phase shift | $\pi$ phase shift | PS | PS |
| First plane | L | 3.63 | −0.66 | 37.37 | 13.85 |
| | T | 4.54 | −0.68 | 36.10 | 16.92 |
| Second plane | P | 4.25 | −0.79 | 14.86 | 8.16 |
| | L | 3.38 | −0.79 | 13.40 | 6.72 |

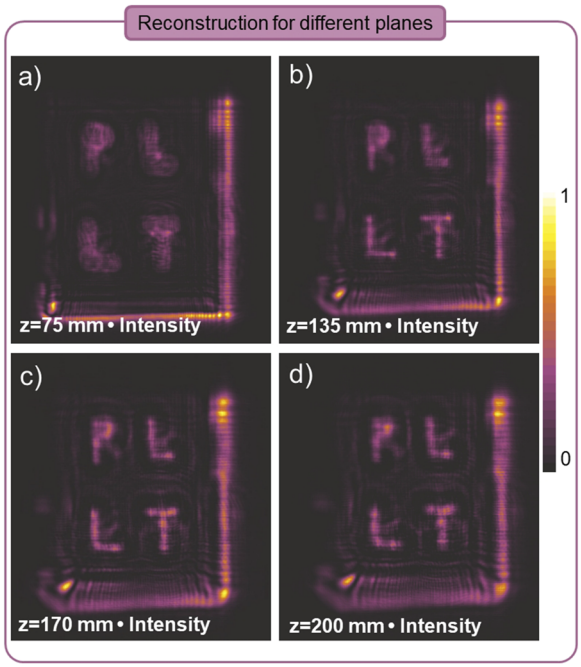


**FIG. 6.** Different reconstruction planes, equal to (a) 75, (b) 135, (c) 170 and (d) 200 mm, reconstructed from the hologram for 600 GHz. For such small hologram size, a large depth of field is observed under illumination with a parallel beam.

One can notice that the size of the recorded hologram is limited to 118 × 138 mm$^2$ for 0.5 and 1 mm wavelengths. The smaller the reconstruction area, the larger the depth of the field. This results in the appearance of the sharp image observed in a wide range of distances. Here, the reconstruction was conducted at distances from the hologram from 30 to 200 mm in 5 mm steps. The image is very similar to that illustrated in Fig. 5, which can be observed from the distance of 75 mm up to 200 mm (further propagation was not performed). This phenomenon can be seen in Fig. 6 where two exemplary more distant planes of the reconstructed hologram are shown. One can see that the letter shape can still be clearly distinguished. If strong inevitable diffraction effects (resulting from the object aperture size, propagation distance, and setup aperture) are not taken into account, the sharp image can be observed not only in one plane but also in the certain range of distances. However, it is difficult to evaluate them numerically even though the human eye sees the difference. Moreover, one needs to recall that in this THz experiment, a plane wave was used both as a reference beam and to illuminate the opaque-transparent object (without the diffuser making the phase random).

## V. RECONSTRUCTION OF THE PHASE SAMPLE (PHASE OBJECT)

A phase object (transparent sample introducing phase changes only) is analyzed by reconstruction with the PS algorithm (both two- and four-step). This is illustrated through a series of measurements of the sample with different numbers of phase shift areas at a frequency of 600 GHz. The reconstruction results using two-step and four-step PS algorithms in the form of the amplitude and phase distributions from the registered holograms are presented in Fig. 7.

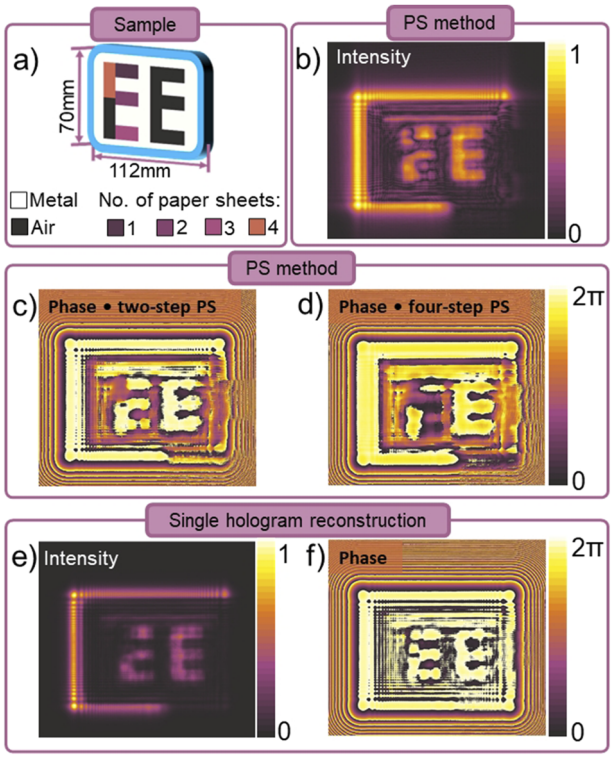


**FIG. 7.** Intensity and phase distributions of the reconstructed holograms. (a) Scheme of the object that consists of a 70 × 112 mm$^2$ aluminum foil with cut-out "EE" shape elements. Note that one of these elements contains areas corresponding to a different number of paper sheets (0, 1, 2, 3, and 4) indicated by different colors (particular phase values) in the image. The relevant intensity and phase distributions of the reconstructed image using the two-step phase-shifting technique are presented in (b) and (c). Additionally, a phase distribution for the four-step PS algorithm is given in (d). The intensity distribution for the four-step technique showed very similar intensity distribution to that of the two-step technique. To illustrate the importance of phase differences, two PS reconstruction algorithms are compared in (c) and (d). For better comparison, the intensity and phase distributions of the reconstructed image using a single hologram are presented in (e) and (f).

The sample, described in Fig. 7(a), was used to illustrate the advantages of using the PS technique. Each additional paper sheet in the reference beam shifts the phase by $\frac{\pi}{4}$. First, the experiment was performed without any paper sheets between M2 and BS2 (Fig. 4), and second, it was repeated by adding 2, 4, and 6 paper sheets, which were intended to shift the phase of the reference THz beam by 0, $\frac{\pi}{2}$, $\pi$, and $\frac{3\pi}{2}$, respectively. The intensity and phase distributions were reconstructed using the two-step PS technique. The results are shown in Figs. 7(b) and 7(c). Additionally, the phase distribution was reconstructed using the four-step PS technique for all recorded holograms [Fig. 7(d)]. The intensity distribution for the four-step technique was very similar to the intensity distribution for the two-step one; thus, it was not plotted additionally here.

As one can see from the results, removing the DC term in the two-step PS technique is faster because it requires only two scans,

while the four-step technique does not give much better results when observing intensity distributions and requires two times longer time to record the holograms. The component corresponding to the virtual image forms only the divergent light field in the real image plane. Thus, it slightly increases the noise level in the background, which does not influence the quality of the reconstructed image significantly.[19] However, in the case of imaging (holography) phase objects, the four-step PS technique should be used due to the fact that it is characterized by better mapping of different phase level areas in the sample.

Figure 8 illustrates the phase levels reconstructed from the recorded holograms—both from simulations and experiment. The calculations show the average values of the phase for each area corresponding to the different numbers of the paper sheets in both "E" letters. Data were taken from simulations carried out in Sec. II for two different cases—with no aperture influence (Fig. 2) and with the small size of the hologram aperture (Fig. 3). These values are gathered on the same plot and compared with the experimental results. Three different techniques are shown—single hologram reconstruction (gray), two-step PS (yellow), and four-step PS (violet). It is worth noting that the particular value of the phase level is not essential; however, the most important item is the tendency between the different areas: As each area introduces different phase shifts, the relation between the following phase shifts should be properly mapped in both simulations and experiment. It can be easily noticed that for single hologram reconstruction (SH), the mapping between the phase shift (number of paper sheets) and the phase level is not linear. The two-step PS technique, both in the simulations and experiment, also does not fulfill the proper mapping between the phase shifts introduced by the object and the calculated phase level. In contrast, the four-step PS exhibits an advantage due to the proper phase mapping.

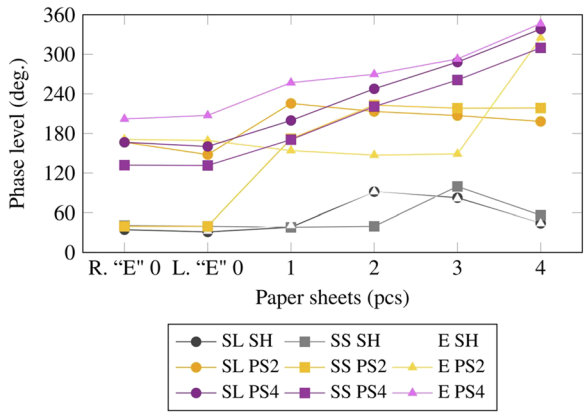


**FIG. 8.** Comparison of phase levels obtained in simulations for large and small apertures of the hologram (SL and SS, respectively) and in experimental evaluation (marked as E). Large aperture simulations correspond to Fig. 2, while phase levels for small apertures are calculated from simulation data illustrated in Fig. 3. Each category—SL, SS, and E—contains information about results obtained from single hologram reconstruction (SH, marked in gray), two-step PS techniques (PS2, marked in yellow), and four-step PS techniques (PS4, marked in red and shifted up by 50° for clarity). It can be seen that the mapping between the numbers of papers, and thus the phase shift introduced by the object, is linearly proportional to phase levels calculated from simulations and experiment only for the four-step PS technique (violet). In the horizontal axis, the numbers of paper sheets are given, which correspond to particular phase shifts introduced by the sample. 16 paper sheets correspond to $2\pi$. "R. "E" 0" and "L. "E" 0" stand for the empty region (0 paper sheet) inside the right and left "E" letter areas, respectively.

## VI. COMPARISON OF PHASE OBJECT IMAGES RECORDED BY DIFFERENT TECHNIQUES

One of the most illustrative ways to reveal the possibilities of phase-imaging applications is to compare the obtained results using different image recording techniques on the same sample. For this purpose, a special sample, i.e., phase object, constructed of differently transparent areas to introduce different phase shifts [Fig. 9(a)], already used in phase-contrast and dark-field imaging experiments,[20] was investigated in addition. Before proceeding to the detailed comparative analysis, it is worth noting the following: In the phase object, almost uniform intensity distribution in the object plane will result in almost uniform intensity distribution in the image plane. Such a problem exists in the $4f$ imaging setup shown in Fig. 9(c); however, this setup allows us to image the whole object plane instantly. To overcome problems with the imaging of phase objects, additional approaches, such as focused imaging [Fig. 9(b)], spatial filtering-based imaging [Fig. 9(d)],[20] or holography, need to be considered. Focused imaging requires raster scanning of the sample (object) plane point-by-point. The spatial filtering technique in the $4f$ setup or holographic approach enables instantaneous THz image formation, i.e., fast acquisition can be realized using a matrix of detectors.

A comparison of the results obtained via the PS technique with previously recorded images using point-to-point, plane-to-plane ($4f$), and dark-field techniques[20] is presented in Fig. 9. One can note the good quality of the intensity image registered using the point-to-point technique [Fig. 9(b)], revealing also some phase differences (edges) that can be registered using the focusing optics. The resolution of the obtained image is in the range of wavelengths. This results from the focal length and the diameter of the used mirror, which influences the Airy disk size in the focal spot. Thus, the smaller the focal spot, the better the resolution. However, in such a case, the point-to-point (raster) scanning is obligatory. To accelerate the imaging process, an array of detectors is needed, but at the same time, it imposes the requirement of different optical setup configurations. The influence of diffraction effects resulting from limited aperture size in comparison to the wavelength[14] forces us to use the large aperture optics to allow for plane-to-plane imaging (like in the $4f$ optical setup). This requirement can be alleviated in some application by using small aperture size optics and shifting the object with the detector placed on the optical axis. This solution can be quickly improved to the plane-to-plane imaging scheme by using large aperture lenses.[21] However, there is one significant drawback—spatial filtering techniques can be applied for objects introducing the phase shifts from the $0–\frac{\pi}{2}$ range. Such limitation results from the theoretical approximation and an assumption that the function describing the object can be expanded into Taylor series. Nevertheless, the holographic imaging can extract the phase values within the range of $0–2\pi$ or even more, but then it requires additional phase retrieval techniques. It should be underlined that using holographic techniques, a complex light field distribution (containing information about the amplitude and phase of the beam) can be extracted at

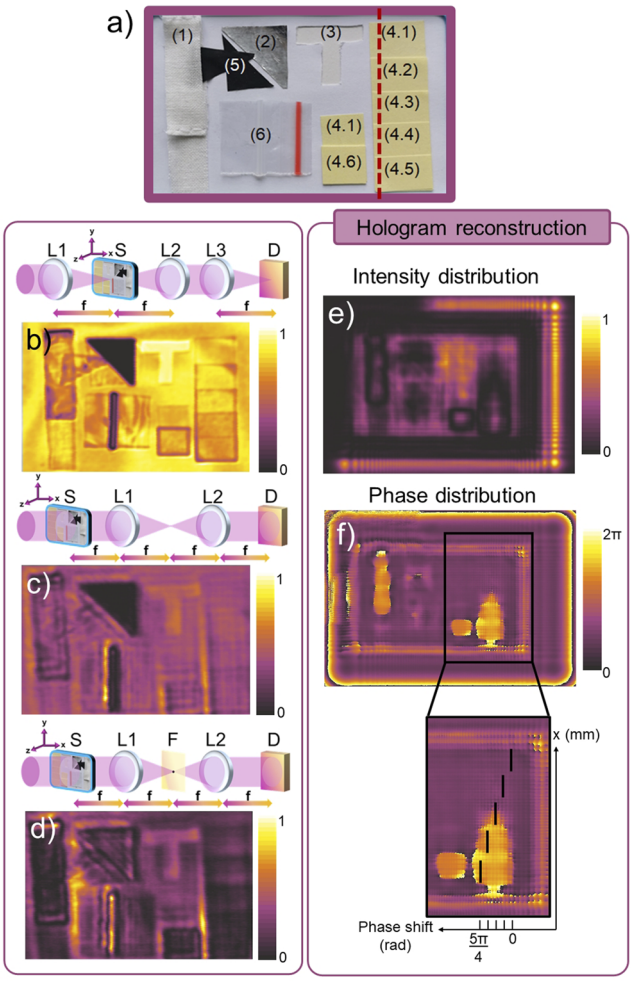


**FIG. 9.** (a) Photograph of the imaged sample consisting of (1) gauze cloth with different numbers of layers, (2) aluminum foil, (3) a T-shaped aperture, (4) paper (where the second number denotes the paper sheet number), (5) rubber glove, and (6) a low density polyethylene (LDPE) bag (two layers of the LDPE film). The comparison of images recorded at 300 GHz by setups described in Ref. 20 with different imaging techniques is shown: (b) direct THz image obtained with focusing THz radiation to the sample and detector—point-to-point technique; (c) direct THz image obtained without focusing THz radiation to the sample and detector—plane-to-plane technique—which is the 4*f* imaging setup; and (d) THz image obtained using the dark-field filtering technique where the spatial filter is used to remove low frequency components from the spectrum, hence allowing us to form the image with a dark background around the sample. (e) and (f) show the intensity and phase distributions, respectively, reconstructed from the registered holograms using the PS technique. The sample part of paper sheets is enlarged in order to see the phase levels. The black lines are given as the guide the eye to indicate the phase change caused by each paper sheet. The hologram was registered and reconstructed for 600 GHz; thus, the phase shift introduced by the same number of paper sheets is two times larger. THz image pixel size: 0.3 × 0.3 mm$^2$; images are of 273 × 165 pixels.

different planes starting from the hologram plane; thus, a 3D light field distribution can be reconstructed.

In Figs. 9(e) and 9(f), the intensity and phase distributions of the reconstructed image are shown. As one can see, the intensity distribution indicates no total transparency in all areas, so the reconstructed intensity is not uniform [Fig. 9(e)]. It is worth to recall that in real experimental conditions, there are no ideally transparent materials; thus, the object under test will introduce some attenuation anyway. Nevertheless, the techniques enabling us to visualize the phase are more adequate due to the fact that they allow us to map different phase values from the object as different phase levels in the image plane. This can be illustrated via the dark-field technique [Fig. 9(d)] and the hologram in the form of reconstructed intensity and phase distributions [Figs. 9(e) and 9(f), respectively]. In Fig. 9(f), the phase distribution reconstructed from the hologram using PS is given with additional zoom in the inset. It can be noticed that in Fig. 9(f), the edges of different areas are visible, and also, the phase level inside the area is distinguishable.

In the case of imaging phase objects, special attention must be given to a proper phase mapping between the phase shift introduced by the object (sample) and the phase value calculated from the image. On the one hand, the average value of the intensity in the areas corresponding to the particular phase shifts was calculated for point-to-point, plane-to-plane, and dark-field techniques. On the other hand, the average value of the phase in the areas corresponding to the particular phase shifts was calculated from phase distribution in the reconstructed hologram. First three methods are supposed to visualize phase changes in the registered intensity pattern. In the fourth method–the hologram—a phase distribution (and amplitude) is reconstructed from the registered intensity interference pattern. These four sets of the data are plotted in Fig. 10, illustrating the dependence of the phase level to the introduced phase shift. It can be clearly seen that there is no proper mapping between the calculated phase level and the introduced phase shifts in the experimentally recorded intensity distributions in the point-to-point and plane-to-plane setups. The dark-field technique (using the amplitude spatial

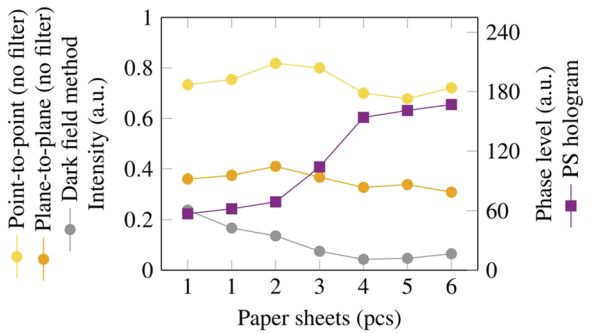


**FIG. 10.** Comparison of different phase level mapping obtained experimentally using different techniques. The intensity patterns are recorded for point-to-point, plane-to-plane, and dark-field techniques—left vertical axis—which are marked as circles in light yellow, dark yellow, and gray colors, respectively. The phase distribution is reconstructed from the hologram and is marked as squares (violet color)—right vertical axis. The dark-field (DF) technique follows the desired change in paper sheet numbers between 1 and 4 (inversely proportional), while the holographic reconstruction follows between paper sheet numbers 1 and 6 (proportionally). It must be underlined that intensity distributions (yellows and gray) were registered for 300 GHz (the $2\pi$ phase shift corresponds to introducing 16 paper sheets), while the hologram (violet) was registered for 600 GHz (the $2\pi$ phase shift corresponds to introducing 8 paper sheets), which give the proper phase mapping range $0–\frac{3\pi}{8}$ for the dark-field technique and $0–\frac{5\pi}{4}$ for the reconstructed hologram.

filter in the middle of the Fourier plane) forms the intensity image of the phase object. However, this object must introduce phase changes up to $\frac{\pi}{2}$, while the larger phase change results in a smaller intensity value in the image. In Fig. 10 (gray dots), the decrease in intensity can be noticed between 1 and 4 paper sheets, which agrees well with the theory and the applicability limits of the dark-field technique.

The hologram reconstruction of the "EE" sample (Fig. 8) revealed the possibility to properly map all introduced 4 paper sheets corresponding to the $0–\pi$ phase change. Here, the 5 paper sheet induced phase difference is properly mapped; however, one can note that the hologram was recorded and reconstructed for shorter wavelengths (higher frequency, 600 GHz). Therefore, the introduced phase shift is equal to $0–\frac{5\pi}{4}$ and is properly mapped with the phase shifts introduced by the sample. Each of the 6 different paper sheet areas (violet squares in Fig. 10) can be distinguished by the comparison of the average value in the reconstructed phase distribution.

## VII. CONCLUSIONS

A two- and four-step PS technique in THz holography is developed, and its ability to reconstruct 2D and 3D transparent objects is demonstrated. The two-step PS technique was found to be faster and easier for application; however, it leaves some divergent light field distribution propagating together with information about the object to the image plane. Therefore, this technique can still influence the phase pattern but cannot give precisely correct mapping between the phase shifts introduced by the sample and the phase levels calculated from the reconstructed hologram.

The four-step PS technique is preferable in the case of determining the exact phase values of the registered phase object. It requires more recording time; however, it exhibits the advantage of the proper phase mapping. For instance, in this article, we demonstrated that within the $0–\frac{5\pi}{4}$ range, the introduced phase changes and distributions can be reconstructed from the hologram using PS techniques.

A comparison of two-step and four-step PS approaches was demonstrated. Purely amplitude objects (not introducing phase variations in the sample plane) can be accurately holographed using the two-step technique, which is two times faster and is characterized with two times larger contrast than single hologram reconstruction. Moreover, the average value of the background in the case of single hologram reconstruction is reduced up to five times when using the two-step PS technique.

To highlight possibilities given by holographic registering of objects and their digital reconstruction, the comparison of the holographic imaging with other methods was given. Holographic imaging gives the information about amplitude and phase distributions in all planes after the hologram, i.e., the complex field can be reconstructed. Another interesting technique—spatial filtering (the dark-field method)—enables the mapping of phase values introduced by the sample into the intensity pattern in the image plane. Such image formation is possible due to the introduction of an amplitude filter in the Fourier plane of the $4f$ optical setup. This method is limited only to the mapping phase changes from the $0–\frac{\pi}{2}$ range. The holographic method can give a phase difference range of $0–2\pi$, and in the case of using additional phase retrieval methods, it is even higher.

The plane-to-plane and point-to-point methods are given as references. The former illustrates how the image is formed in a typical $4f$ setup by suppressing diffraction effects arising from the limited aperture of optical elements by placing the detector in the middle of the optical axis and shifting the sample in the object plane. This method does not provide proper information about the phase levels introduced by the sample. The latter describes the raster scanning method using a focused beam—on both the sample and the detector. This method displays good resolution resulting from the size of the focal spot illuminating the sample. It enhances edges and small changes in the sample. However, it does not provide proper mapping of the phase introduced by the sample with registered intensity values.

To summarize, the holographic methods of imaging give the whole variety of possibilities of forming reconstructed images and visualizing both amplitude and phase changes introduced by the sample. Only in the case of phase reconstruction from the in-line digital hologram using the four-step PS technique, the different phase level areas can be discriminated, indicating that the boundaries of THz imaging and digital holography[22] can be extended, in particular in the application of imaging of phase objects transparent for this particular range of radiation.

## ACKNOWLEDGMENTS

This study was funded by the FOTECH-1 project granted by the Warsaw University of Technology under the program Excellence Initiative: Research University (ID-UB).

The authors acknowledge Orteh Company for providing LS 6.0 software used here for the numerical reconstruction of the recorded holograms, which is accessible in the Laboratory of Optical Information Processing at the Faculty of Physics in the Warsaw University of Technology.

## AUTHOR DECLARATIONS

### Conflict of Interest

The authors have no conflicts to disclose.

## DATA AVAILABILITY

The data that support the findings of this study are available from the corresponding author upon reasonable request.

## APPENDIX: SINGLE HOLOGRAM RECONSTRUCTION

To compare the hologram reconstruction using the PS technique and the simple hologram reconstruction for 300 GHz, one needs to analyze the reconstructed images from the hologram recorded with no phase shift in the reference arm and with the $\pi$ phase shift. Such a phase shift was realized by four layers of paper, glued together, and introduced in the reference arm. It can be seen that reconstructed two-plane-images [Figs. 11(e) and 11(f)] for both holograms have inverted contrast (violet) in relation to those in Figs. 11(a) and 11(b) resulting from the recording with $\pi$-shifted reference beams. The phase distribution seems to be more uniform and thus less distinguishable than for the PS technique (illustrated in

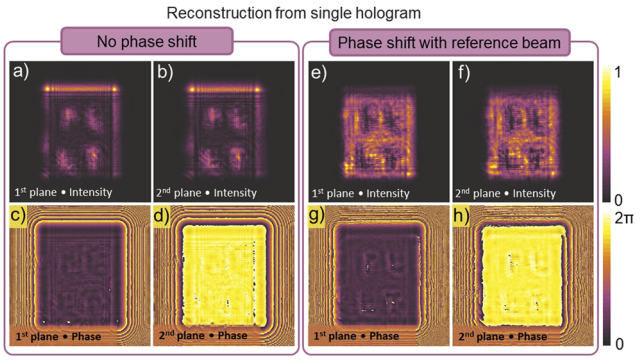


**FIG. 11.** Amplitude (a, b, e, and f) and phase (c, d, g, and h) distributions of reconstructed images for both planes for each hologram separately for 300 GHz (single hologram reconstructions). (a)–(d) Without the phase shift introduced in the reference arm and (e)–(h) with the $\pi$ phase shift introduced.

Fig. 5). The quantitative comparison of single hologram reconstructions with the one using the two-step PS technique is described in Sec. V.

## REFERENCES

[1]L. Guo, X. Wang, and Y. Zhang, "Terahertz digital holographic imaging of biological tissues," in *International Symposium on Ultrafast Phenomena and Terahertz Waves* (Optical Society of America, 2016), p. IW4B-3.
[2]L. Guo, X. Wang, P. Han, W. Sun, S. Feng, J. Ye, and Y. Zhang, "Observation of dehydration dynamics in biological tissues with terahertz digital holography," Appl. Opt. **56**, F173–F178 (2017).
[3]L. Rong, T. Latychevskaia, D. Wang, X. Zhou, H. Huang, Z. Li, and Y. Wang, "Terahertz in-line digital holography of dragonfly hindwing: Amplitude and phase reconstruction at enhanced resolution by extrapolation," Opt. Express **22**, 17236 (2014); arXiv:0911.0520.
[4]Z. Li, R. Zou, W. Kong, X. Wang, Q. Deng, Q. Yan, Y. Qin, W. Wu, and X. Zhou, "Terahertz synthetic aperture in-line holography with intensity correction and sparsity autofocusing reconstruction," Photonics Res. **7**, 1391 (2019).
[5]H. Yuan, A. Lisauskas, M. Wan, J. T. Sheridan, and H. G. Roskos, "Resolution enhancement of THz imaging based on Fourier-space spectrum detection," Proc. SPIE **11279**, 1127918 (2020).
[6]S. T. Thurman and A. Bratcher, "Multiplexed synthetic-aperture digital holography," Appl. Opt. **54**, 559 (2015).
[7]M. S. Heimbeck and H. O. Everitt, "Terahertz digital holographic imaging," Adv. Opt. Photonics **12**, 1–59 (2020).
[8]I. Yamaguchi and T. Zhang, "Phase-shifting digital holography," Opt. Lett. **22**, 1268–1270 (1997).
[9]T. Zhang and I. Yamaguchi, "Three-dimensional microscopy with phase-shifting digital holography," Opt. Lett. **23**, 1221–1223 (1998).
[10]C. Zuo, S. Feng, L. Huang, T. Tao, W. Yin, and Q. Chen, "Phase shifting algorithms for fringe projection profilometry: A review," Opt. Lasers Eng. **109**, 23–59 (2018).
[11]D. W. Phillion, "General methods for generating phase-shifting interferometry algorithms," Appl. Opt. **36**, 8098–8115 (1997).
[12]G. Lai and T. Yatagai, "Generalized phase-shifting interferometry," J. Opt. Soc. Am. A **8**, 822–827 (1991).
[13]L. Xu, J. Miao, and A. K. Asundi, "Properties of digital holography based on in-line configuration," Opt. Eng. **39**, 3214–3219 (2000).
[14]A. Siemion, "The magic of optics—An overview of recent advanced terahertz diffractive optical elements," Sensors **21**, 100 (2021).
[15]L. Minkevičius, L. Qi, A. Siemion, D. Jokubauskis, A. Sešek, A. Švigelj, J. Trontelj, D. Seliuta, I. Kašalynas, and G. Valušis, "Titanium-based microbolometers: Control of spatial profile of terahertz emission in weak power sources," Appl. Sci. **10**, 3400 (2020).
[16]G. Dwivedi, A. Sharma, S. Debnath, and Rajkumar, "Comparison of numerical reconstruction of digital holograms using angular spectrum method and Fresnel diffraction method," J. Opt. **2017**, 1–10 (2017).
[17]M. Sypek, "Light propagation in the Fresnel region. New numerical approach," Opt. Commun. **116**, 43–48 (1995).
[18]M. S. Heimbeck, W.-R. Ng, D. R. Golish, M. E. Gehm, and H. O. Everitt, "Terahertz digital holographic imaging of voids within visibly opaque dielectrics," IEEE Trans. Terahertz Sci. Technol. **5**, 110–116 (2014).
[19]A. Siemion, I. Ducin, K. Kakarenko, M. Makowski, A. Siemion, J. Suszek, M. Sypek, D. Wojnowski, and A. Kołodziejczyk, "Digital holography with self-imaging by a two-step phase element," Photonics Lett. Pol. **2**, 91–93 (2010).
[20]A. Siemion, L. Minkevičius, L. Qi, and G. Valušis, "Spatial filtering based terahertz imaging of low absorbing objects," Opt. Lasers Eng. **139**, 106476 (2021).
[21]M. Sypek, M. Makowski, E. Hérault, A. Siemion, A. Siemion, J. Suszek, F. Garet, and J.-L. Coutaz, "Highly efficient broadband double-sided Fresnel lens for THz range," Opt. Lett. **37**, 2214–2216 (2012).
[22]G. Valušis, A. Lisauskas, H. Yuan, W. Knap, and H. G. Roskos, "Roadmap of terahertz imaging 2021," Sensors **21**, 4092 (2021).